VFAST Transactions on Mathematics
http://vfast.org/journals/index.php/VTM@ 2023, ISSN(e): 2309-0022, ISSN(p): 2411-6343
Volume 11, Number 1, January-June, 2023 *pp: 217-236*

Numerical analysis of flow rates, porous media, and Reynolds numbers affecting the combining and separating of Newtonian fluid flows

Rahim Bux Khokhar[1], **Afaque Ahmed Bhutto**[2*], **Noor Fatima Siddiqui**[3], **Fozia Shaikh**[1], **Iftikhar Ahmed Bhutto**[4]

[1]BSRS Department MUET, Jamshoro, Pakistan; [2*]BSRS Department, QUEST, campus Larkana, Pakistan; [3]Department of Mathematics, University of Karachi, Pakistan; [4]Sukkur IBA University, Sukkur, Pakistan

Keywords: *Newtonian fluids, vortex intensity, Reynolds number, flow rate, inertia, Porous media.*
Subject Classification: *Numerical technique, Modeling, and Simulation.*
Journal Info:
Submitted:
May 01, 2023
Accepted:
June 15, 2023
Published:
June 30, 2023

Abstract This study investigates the behavior of Newtonian fluids in pipes filled with and without porous media under combing and separating flow configurations. Numerical simulations are conducted to analyze the effects of changing flow rates, inertia, and porous media on flow patterns, vortex development, and pressure difference. The aim of this study is to examine the impact of inertia on flow behavior by analyzing the streamline patterns, vortex growth, and intensity at different Reynolds numbers, ranging from Re=1 to Re=5000.

***Correspondence Author Email Address:**
afaq_bhutto@quest.edu.pk

1 Introduction

The numerical simulations and analysis of fluid flow within a channel filled with non-porous media. Understanding the behavior of fluid flows and the associated pressure variations is essential in various engineering and scientific applications [1, 2]. The effects of inertia on flow patterns and pressure are of particular interest. Inertia plays a crucial role in determining the movement and behavior of fluid within the channel.

By varying the Reynolds number, which is a dimensionless parameter representing the ratio of inertial forces to viscous forces, we can analyze the impact of inertia on the observed flow patterns and pressure differences [3–6]. The study of flows in channels has great importance due to its widespread applications in various industries such as chemical, biomedical, and mechanical engineering. The behavior of Newtonian fluids in channels is characterized by the presence of unidirectional and reverse flows. Understanding the dynamics of such flows is critical to optimizing fluid transportation processes and reducing energy consumption [3, 7–9]. Over the past half-century, the study of smooth fluid movement through intricate channels and pipes containing porous and non-porous materials has remained a crucial and intriguing topic in the field of CFD, particularly in various processing industries [7, 10–12]. Due to the intricate flow behavior of non-linear fluids, which exhibit convoluted rheological properties, and the intricacy of the domains involved, industrial issues become more challenging to tackle. Hence, these complexities stimulate and challenge mathematicians and scientists. There are several industrial scenarios discussed in the paper, but the author places emphasis on only a few. There are industries that process crude oil, enhanced oil recovery within the petroleum sector, ceramics, chemicals, cosmetics, dryers, filters, food, and pharmaceuticals. The author [13] also discusses a number of reactors related to the aforementioned applications. Several studies have investigated the behavior of unidirectional and reverse flows of Newtonian fluids in channels [2]. Experimentally investigating the characteristics of the single-dimensional flow of a linear fluid in a rectangular channel, the authors found that the velocity profiles of the flow were well described by the laminar flow theory [14]. Further, Afonso [1] investigated the behavior of reverse flows in a horizontal channel. He found that the reverse flow was initiated by a small disturbance near the inlet and then developed into a stable vortex. Incompressible laminar flows of fluids are a fundamental problem in fluid mechanics that has been studied for decades. The behavior of these flows in complex domains, which can include obstacles, corners, and curved surfaces, is of specific interest due to its significance to many real-world applications [15, 16]. Porous media can also significantly affect the behavior of fluid flows, and understanding the interactions between fluids and porous media is crucial in fields such as geology, environmental engineering, and oil extraction.

The study explores the behavior of incompressible laminar fluid flows within intricate domains, both with and without porous media [2, 3, 17]. Over the past few decades, progress in state-of-the-art, rapid computing systems has progressed significantly, resulting in the creation of intricately designed numerical algorithms. The practical application of computer simulations to analyze complicated fluid dynamics within a domain containing permeable materials has been widely acknowledged and further enhanced by global institutions [18]. The Computational Fluid Dynamics (CFD) approach is expected to exhibit a particular characteristic owing to its ability to perform constraint-based simulations. Over the last three decades, there has been significant progress in enhancing our knowledge of numerical uncertainties, and the flow nature, such as unsteady, and turbulence [19]. The mathematical modeling of flow behavior by mixing and separating simultaneously, as well as other modifications, was first initiated by Cochrane et al.,[20] and was experimentally and numerically solved using the finite difference method. Baloch [3] conducted a few 2D analyses using the finite element algorithm, and Afonso [21] used the finite volume technique. Mixing and separation in rectangular channels and pipes, whether filled with porous media or not, exhibit a plethora of captivating flow phenomena. These include the appearance of singularities at acute bends and the formation of flow transition. These diverse flow phenomena occur within the same domain, as observed by Cochrane [20], Dharejo [22], Khokhar [4], Afonso [21], and Echendu [2]. Baloch [3] investigated the mixing and separating flow of highly elastic fluids using a time-dependent finite element technique.

Taylor-Petrov-Galerkin algorithms were utilized due to the elastic nature of the fluids [23]. Further, he used the pressure-correction method to achieve second-order accuracy in incompressibility. The researchers simulated Newtonian fluid flow with equal flow rates in both arms, while they simulated viscoelastic flows with the Phan-Thien and Tanner (PTT) constitutive model [24], which numerically illustrates shear-thinning behavior and the effect of changing in space between plates. They studied various physical parameters, and flow situations [25]. According to Afonso [1], even creeping flow or limited vanishing inertia can reduce the inertia effect on the flow rate. A recent study [26] used numerical simulations in the same flow domain to study linear and viscoelastic liquids. The study begins by examining different flow configurations, including reversed and unidirectional flows. These configurations are characterized by specific inlet and outlet placements within the channel. Through numerical simulations, we explore the behavior of fluid flows, the formation of vortices, and the influence of flow rates on pressure distribution.

The aim of the study is to investigate the behavior of Newtonian fluids in pipes under combing and separating flow configurations, both with and without the presence of porous media. The study aims to understand the effects of changing flow rates, inertia, and Darcy's number on flow patterns, vortex development, and pressure distribution within the computational domain. Further to compare the results obtained from different flow conditions, such as equal and unequal flow rates, and analyze the influence of varying values of permeability on the system.

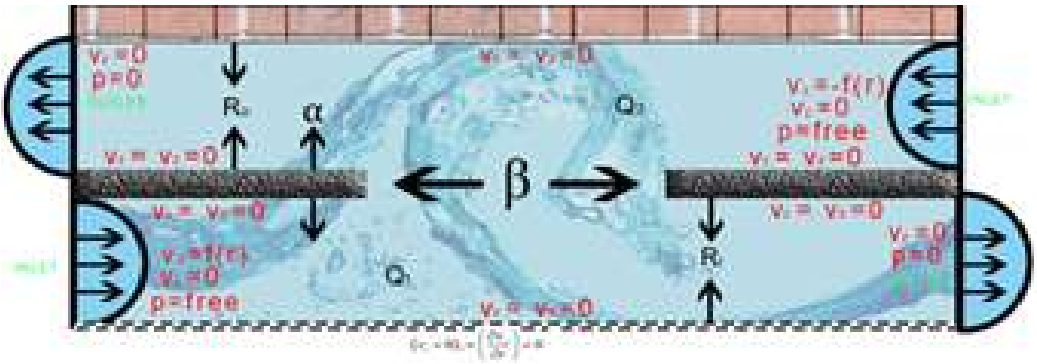

(a) Fluid mixing and separation in a cylindrical pipe

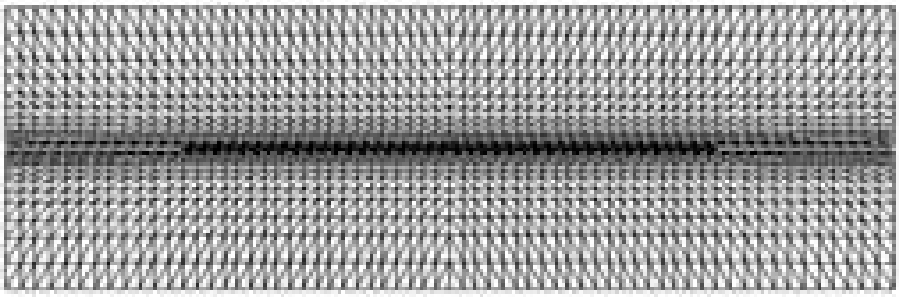

(b) Mesh used in the simulation is a finite element mesh

Figure 1. Geometrical parameters of the computational domain and mesh.

2 Problem specification

The study focuses on the flow behavior in a combined pipe-cylinder system, where fluid flows through an inner pipe and an outer cylinder, creating a mixing and separating phenomenon in the central gap. The geometry consists of a circular tube with two-dimensional axial and radial directions, and the fluid type can be the same or different by varying the Reynolds number. The inner pipe has a radius of R_i the outer pipe has a radius of R_0, and α = 0.0245 represents the non-dimensional thickness of the inner pipe. The research investigates the flow of Newtonian fluids with and without porous media in the combined system, utilizing a mesh structure shown in Figure 1(b), with a total of 5049 elements, 19057 nodes, and 73953 degrees-of-freedom. Here are the fundamental dimensionless equations that govern a fluid with a variable viscosity that is in motion in an incompressible state and finite conductivity in a steady state, under the influence of a magnetic field:

3 Governing system of equations

In a porous medium filled with non-porous pipes, Newtonian fluids move in two dimensions and at isothermal temperatures. Newtonian fluid transport equations, considering boundary conditions, expressed in cylindrical polar coordinates as follows:

$$\frac{\partial v_z}{\partial z} + \frac{1}{r}\frac{\partial (r v_r)}{\partial r} = 0, \tag{1}$$

Equations of Darcy-Brinkman neglecting body forces at the component level. r–component:

$$\rho\left(\frac{\partial v_r}{\partial t} + v_r\frac{\partial v_r}{\partial r} + v_z\frac{\partial v_r}{\partial z}\right) = \mu\left[\frac{1}{r}\frac{\partial}{\partial r}\left(r\frac{\partial v_r}{\partial r}\right) - \frac{v_r}{r^2} + \frac{\partial^2 v_r}{\partial z^2}\right] - \frac{\partial p}{\partial r} - \frac{\mu}{\kappa}v_r, \tag{2}$$

z–component:

$$\rho\left(\frac{\partial v_z}{\partial t} + v_r\frac{\partial v_z}{\partial r} + v_z\frac{\partial v_z}{\partial z}\right) = \mu\left[\frac{1}{r}\frac{\partial}{\partial r}\left(r\frac{\partial v_z}{\partial r}\right) + \frac{\partial^2 v_z}{\partial z^2}\right] - \frac{\partial p}{\partial z} - \frac{\mu}{\kappa}v_z, \tag{3}$$

The axial and radial components of velocity, isotropic pressure, the density of the fluid, the viscosity of a fluid, and permeability of porous media are represented as $v_z, v_r, p, \rho, \mu, and \kappa$. If both equations (2) and (3) are nonporous.

3.1 The Non-Dimensional System of Equations

We introduce specific dimensionless variables to express the governing equations in a non-dimensional form:

$$r^* = \frac{r}{R_c}, z^* = \frac{z}{R_c}, v_r^* = \frac{v_r}{R_c}, \kappa = \kappa^* R_c^2\frac{v_z}{V_c}, t^* = \frac{t * v}{R_c}, p^* = \frac{p}{\rho V_c^2}$$

According to the equation, V_c is the characteristic velocity of the pipe, and R_c is its length. The velocity of the fluid is taken to be V_c, while the radius of the inner pipe is taken to be R_c. The system of Equations (1 - 3) can be simplified and shortened by substituting the non-dimensional values in Equations (2 - 3):

$$\frac{\partial v_z}{\partial z} + \frac{1}{r}\frac{\partial (r v_r)}{\partial r} = 0, \tag{4}$$

$$\frac{\partial v_r}{\partial t} + v_r\frac{\partial v_r}{\partial r} + v_z\frac{\partial v_r}{\partial z} = -\frac{\partial p}{\partial r} + \frac{1}{Re}\left(\frac{\partial^2 v_r}{\partial r^2} + \frac{1}{r}\frac{\partial v_r}{\partial r} + \frac{\partial^2 v_r}{\partial z^2} - \frac{v_r}{r^2}\right) - \frac{1}{ReD_\alpha}v_r, \tag{5}$$

$$\frac{\partial v_z}{\partial t} + v_r \frac{\partial v_z}{\partial r} + v_z \frac{\partial v_z}{\partial z} = -\frac{\partial p}{\partial z} + \frac{1}{Re}\left(\frac{\partial^2 v_z}{\partial r^2} + \frac{1}{r}\frac{\partial v_z}{\partial r} + \frac{\partial^2 v_z}{\partial z^2}\right) - \frac{1}{ReD_\alpha} v_z, \tag{6}$$

Where D_α is Darcy's number and Re is a Reynolds number:

$$Re = \frac{\rho V_C R_C}{\mu} \quad and \quad D_\alpha = \frac{\kappa}{R_C^2}. \tag{7}$$

3.2 Initial and boundary conditions

To accomplish the problem requirement, it needed to set initial and boundary conditions. Equation (12) extended by boundary condition specified as:

$$v(z, 0) = v_0(z)$$

Subject to

$$\nabla . v_0 = 0$$

With quiescent initial conditions, the velocity vector field and pressure are simulated. Disappearing values of the velocity vector and pressure used in the simulations, along with tractions-free velocity components ($v_r = v_z = p = 0$).

Figure 1(a) illustrates that boundary conditions are fundamental to the simulation of well-posed problems. The domain exit is normally traction-free when the pressure datum is zero. In this case, $v_r = v_z = 0$ represents no-slip boundary conditions. On the axis of symmetry, Neumann conditions are executed ($v_r = 0, \frac{\partial v_z}{\partial r} = 0$). As fluid flows through a pipe, Inlet velocity profiles fully developed before flow begins. At the inlet of a pipe, the non-dimensional analytic solution and the axial velocity are defined without cross-flow. Both inlets, whether they are on the inner or outer pipe, are subject to the following boundary conditions:

$$v_z = V_1(1 - r^2) \quad (Inletleftofinnerpipe), \tag{8}$$

$$v_z = V_2(r - a)(b - r) \quad (Right \quad inlet \quad of \quad outer \quad cylinder). \tag{9}$$

Where, V_1 and V_2 are maximum velocities based on flow rate, $a = R_i + \alpha$ (During the geometry, $\alpha = 0.0254L$ represents the thickness of the inserted plate) and $b = R_0$. The axial and radial coordinates of an axisymmetric flow velocity, vector field are v_r and v_z. The maximum velocities in the center of a domain are equal ($V_1 = V_2,$) in the case of equal flow rates. When the flow rate V_1 and V_2 is unequal, fluid is taken in the ratio of 1:2. During the mesh design, the minimum element size is selected near a separation of 0.003. Figure 1(b) illustrates a finite element mesh on the domain, where the total number of elements, nodes, boundary nodes, and vertex nodes are 1328, 2853,392,763.

4 Numerical scheme

The Navier-Stokes equations and the constraint of incompressibility were simulated using a semi-implicit time-stepping method. The Taylor-Galerkin/Pressure-Correction finite element method is employed in this simulation approach. Using time-marching algorithms, we are able to obtain highly accurate results for both transient and steady flow problems [27]. The Taylor-Galerkin algorithm we use is a fractional-step method that discretizes the problem into two steps: first in the temporal domain, and then in the spatial domain by means of Taylor series expansion. With this approach, we are able to achieve a second-order

time-stepping scheme through a two-step Lax-Wendroff approach and a pressure correction procedure. A spatial Galerkin finite element method is used for spatial discretization. Using this method, velocity is approximated using quadratic basis functions, while pressure is approximated using linear basis functions. It is important to note that this choice of basis functions ensures that the Babuka-Brezzi conditions are satisfied, which is important in order to avoid spurious oscillations in the pressure field [28] and [29].

4.1 Taylor–Galerkin/Pressure–Correction Scheme

The Taylor-Galerkin scheme's primary objective formulates an efficient and highly accurate time-stepping scheme to capture both transient and steady-state solutions of fluid flow problems. Originally, Donea [27] presented the algorithm to handle the time-dependent flows of Newtonian liquids while treating the incompressibility condition implicitly. The procedure employs Taylor series expansions to achieve temporal discretization. A two-step predictor-corrector scheme using Lax-Wendroff approximation was used for second-order temporal accuracy of results. The algorithm also captures greater-order accuracy for time derivatives and reliable spatial derivatives. Compared to Euler-Galerkin and Finite Difference methods, the algorithm demonstrates a significant improvement in accuracy and stability [23, 27].

The Pressure-correction/projection method is a numerical technique originally suggested by Chorin [30] and later refined by Fortin [13]. It separates the pressure and velocity fields and uses a linearized momentum analysis to achieve generally second-order accuracy and stability [31, 32]. This method has since evolved into a variety of related techniques, such as the TGPC algorithm [33, 34], which is the numerical algorithm employed in this research. Similar approaches associated with finite difference research work can also be found [3, 35, 36]. More detailed information on the transient flows of Newtonian fluids [2, 23] can be consulted. However, when it comes to non-Newtonian fluids, the algorithm has extended experimentally and numerically in both semi-implicit and fully implicit forms. For flows that are diffusion dominant, the semi-implicit algorithm has proven to be both numerically accurate and computationally efficient, making it a stable choice for specific problems. In the proposed study, the semi-implicit type of the TGCP algorithm is applied, and thus, the aforementioned approach is demonstrated here.

4.2 Semi–implicit time–stepping scheme

A semi-implicit time-stepping method is a numerical approach operated to solve partial differential equations (PDEs) that contain stiff and non-stiff terms. Using three Jacobi mass-matrix iterations, this method aims to obtain exact results. When implementing a semi-implicit method for Newtonian problems, typical time steps are $\Delta t \leq 0.1$. According to references [37, 38], steady-state solutions should be achieved by allowing a relative increment tolerance of 10^{-1} times the time step.

4.3 Cylindrical polar coordinates

In numerical simulation, the selection of an algorithm depends upon a number of factors, including accuracy, convergence rate, efficiency, and stability. Several studies have demonstrated that semi-implicit methodologies have better convergence rates than explicit methodologies [3, 35, 37, 39]. Generally, implicit techniques are used to enhance numerical stability without incurring excessive computational costs. These are the specifics of the discrete semi-implicit equations, which involve Darcy's component. Stage–1(a):

$$\left[\frac{2}{\Delta t}M + \frac{1}{Re}\left(\frac{S_{rr}}{2} + \frac{M}{D_\alpha}\right)\right]\left(V_{r,j}^{n+\frac{1}{2}} - V_{r,j}^{n}\right) = \left[-\frac{1}{Re}(S_{rr} + S_{rz})V_{r,j} - J_1^t P_k\right]^n - N(V)V_{r,j}^n - \frac{1}{ReD_\alpha}MV_{z,j}^n, \tag{10}$$

$$\left[\frac{2}{\Delta t}M + \frac{1}{Re}\left(\frac{S_{zz}}{2} + \frac{M}{D_\alpha}\right)\right]\left(V_{z,j}^{n+\frac{1}{2}} - V_{z,j}^{n}\right) = \left[-\frac{1}{Re}(S_{rz}^t + S_{zz})V_{z,j} - J_2^t P_k\right]^n - N(V)V_{z,j}^n - \frac{1}{ReD_\alpha}MV_{z,j}^n, \tag{11}$$

Stage–1(b):

$$\left[\frac{1}{\Delta t}M + \frac{1}{Re}\left(\frac{S_{rr}}{2} + \frac{M}{D_\alpha}\right)\right]\left(V_{r,j}^{*} - V_{r,j}^{n}\right) = \left[-\frac{1}{Re}(S_{rr} + S_{rz})V_{r,j} - J_1^t P_k^n\right]^n - N(V)V_{r,j}^{n+\frac{1}{2}} - \frac{1}{ReD_\alpha}MV_{r,j}^n, \tag{12}$$

$$\left[\frac{1}{\Delta t}M + \frac{1}{Re}\left(\frac{S_{zz}}{2} + \frac{M}{D_\alpha}\right)\right]\left(V_{z,j}^{*} - V_{z,j}^{n}\right) = \left[-\frac{1}{Re}(S_{rz}^t + S_{zz})V_{z,j} - J_2^t P_k^n\right]^n - N(V)V_{z,j}^{n+\frac{1}{2}} - \frac{1}{ReD_\alpha}MV_{z,j}^n, \tag{13}$$

Stage–2:

$$K(Q^{n+1}) = -\frac{2}{\Delta t}(J_1 V_{r,j} + J_2 V_{z,j}), \tag{14}$$

Stage–3:

$$M(V_{r,j}^{n+1} - V_{r,j}^{*}) = \frac{\Delta t}{2}J_1^t(p^{n+1} - p^n), \tag{15}$$

$$M(V_{z,j}^{n+1} - V_{z,j}^{*}) = \frac{\Delta t}{2}J_2^t(p^{n+1} - p^n), \tag{16}$$

$S = \int\left(\frac{\partial\phi_i}{\partial x}\frac{\partial\phi_j}{\partial x} + \frac{\partial\phi_i}{\partial y}\frac{\partial\phi_j}{\partial y}\right)d\Omega$is a momentum diffusion matrix, $J = (J_1, J_2)$ and $K = \int\left(\frac{\partial\psi_{ki}}{\partial x}\frac{\partial\psi_{kj}}{\partial x} + \frac{\partial\psi_{ki}}{\partial y}\frac{\partial\psi_{kj}}{\partial y}\right)d\Omega$ represent a pressure stiffness, $J_1 J_2$ are divergence pressure gradient, V^n, V^*, V^{n+1} are nodal vectors of the velocity field, p^n, p^{n+1} is a pressure, t transpose matrix, and Δt is the time interval (t_n, t_{n+1}). V_j^n, is a nodal velocity vector at time t_n, V_j^* is an intermediate non-divergence-free velocity vector and V_j^{n+1} is a divergence-free velocity vector at time step t_{n+1}, p_k^n is a pressure vector and $Q^{n+1} = p_k^{n+1} - p_k^n$ is a pressure difference vector.

4.4 Finite Element Discretization

A variational formulation consuming a weighted approach along with a finite element approximation is used to discretize the aforementioned set of equations (21 - 24) in the spatial domain. The objective of this approach is to represent the equations in a form that allows for numerical approximation. The shape and weight functions defined in Hilbert spaces that are subsets of the two-dimensional Euclidean space $\Omega \subset R^2$. Specifically, we consider the Hilbert space $H^1(\Omega)^2$ for scalar-valued functions and their first-order derivatives, and the vector-valued Sobolev space for functions, which are integrable squares in the $L^2(\Omega)$ norm with their second-order derivatives. Finite element approximation is based on these function spaces. With the purpose of obtaining an inclusive interpretation of the precise definitions of these function spaces, the interested reader should refer to references [3] and [37]. The approach outlined above represents a standard methodology for discretizing and approximating the equations in question.

$$V = \left(u^n \subset H^1(\Omega)^2 \mid u\Gamma_1^n = b\right), \tag{17}$$

$$V_0 = \left(v \subset H^1(\Omega)^2 \mid u\Gamma_1 = 0\right). \tag{18}$$

For integrable square functions, the traditional inner–product exemplification is described as:

$$< f, g >= \int_\Omega f(x)g(x)d\Omega. \tag{19}$$

Let $L^2(\Omega)$be the Hilbert space for square-integrable functions:

$$P = (q \subset L^2(\Omega)^d). \tag{20}$$

The following semi-discrete variational forms are predicted at different stages: Stage–1a:

$$\left(\left(\frac{2}{\Delta t} - \frac{1}{2Re}\nabla^2 + \frac{1}{2ReD_\alpha}\right)\left(v^{n+\frac{1}{2}} - v^n, v\right)\right) = \left(\frac{1}{Re}\nabla^2 v - (v.\nabla)v - \frac{1}{ReD_\alpha}v, v\right) - (\nabla p, q), \tag{21}$$

Stage–1b:

$$\left(\left(\frac{1}{\Delta t} - \frac{1}{2Re}\nabla^2 + \frac{1}{ReD_\alpha}\right)(v^* - v^n, v)\right) = \left(\frac{1}{Re}\nabla^2 v - \frac{1}{ReD_\alpha}v, v\right)^n - (\nabla p, q)^n - \left(v.\nabla v^{n+\frac{1}{2}}, v\right) \tag{22}$$

Stage–2:

$$\theta\nabla^2(p^{n+1} - p^n, q) = \frac{1}{\Delta t}(\nabla.v^*, v), \tag{23}$$

Stage–3:

$$\frac{2}{\Delta t}(v^{n+1} - v^*, v) = -\nabla(p^{n+1} - p^n, q). \tag{24}$$

To develop a discrete scheme of the problem, which defines proper finite-dimensional subspaces of and respectively. By using the weighted residual technique, the above equation (20) is spatially discretized using the Galerkin approximation method, in which the weight function is reserved to be equivalent to the shape function. The shape functions consumed for determining velocity and pressure components are piecewise quadratics and piecewise linear over triangular mesh tessellations, respectively. We introduce the approximate solutions of primitive variables, u(x,y,t),v(x,y,t) and p(x,y,t), over finite spaces of the following functions:

$$u(x, y, t) \cong \Sigma_{j=1}^{6} U_j^n(t)\Phi_j(x, y), \tag{25}$$

$$v(x, y, t) \cong \Sigma_{j=1}^{6} V_j^n(t)\Phi_j(x, y), \tag{26}$$

$$p(r, z, t) \cong \Sigma_{k=1}^{3} P_k(t)\psi_k(r, z), \tag{27}$$

Here, ψ_k and Φ_j are linear and quadratic shape functions respectively. Equations (21 to 24) symbolizations are followed [4]. The compact matrix form of the discrete system is: Stage–l a:

$$\left[\left(\frac{2M}{\Delta t} - \frac{1}{Re}\left(\frac{S}{2} + \frac{M}{D_\alpha}\right)\right)\left(V^{n+\frac{1}{2}} - V^n\right) = \left[-\frac{1}{Re}(SV_j) + j_1^t P_k - N(V)V_j - \frac{1}{ReD_\alpha}MV_j\right]\right]^n, \tag{28}$$

Stage–l b:

$$\left[\frac{M}{\Delta t} - \frac{1}{Re}\left(\frac{S}{2} + \frac{M}{D_\alpha}\right)\right](V^* - V^n) = \left[-\frac{1}{Re}(SV_j) + j_2^t P_k - \frac{1}{ReD_\alpha}MV_j\right]^n - N(V)V_j^{n+\frac{1}{2}}, \tag{29}$$

Stage–2:

$$K(p^{n+1} - p^n) = -\frac{2}{\Delta t}JV_j^*, \tag{30}$$

Stage–3:

$$\frac{2M}{\Delta t}(V_j^{n+1} - V_j^*) = J^t(p^{n+1} - p^n). \tag{31}$$

Where, $M = int\Phi_i\Phi_j d\Omega$ is a consistent mass matrix, $N(V) = \int\left(\Phi_i(\Phi_l U_l)\frac{\partial\Phi_j}{\partial x} + \Phi_i(\phi_l V_l)\frac{\partial\Phi_j}{\partial y}\right)d\Omega$ is a convection matrix, $S = \int\left(\frac{\partial\Phi_i}{\partial x}\frac{\partial\Phi_j}{\partial x} + \frac{\partial\Phi_i}{\partial y}\frac{\partial\Phi_j}{\partial y}\right)d\Omega$ is a momentum diffusion matrix, $J_1 = \int\frac{\partial\Psi_i}{\partial x}\Phi_j d\Omega$ and $J_2 = \int\frac{\partial\Psi_i}{\partial y}\Phi_j d\Omega$ are divergence/pressure gradient matrix and $J = (J_1, J_2)$ and $K = \int\left(\frac{\partial\Psi_{ki}}{\partial x}\frac{\partial\Psi_{kj}}{\partial x} + \frac{\partial\Psi_{ki}}{\partial y}\frac{\partial\Psi_{kj}}{\partial y}\right)d\Omega$ is a pressure stiffness matrix. Here, t is the transpose of a matrix, p^n, p^{n+1} is pressure, V^n, V^*, V^{n+1} are nodal vectors of the velocity field, and Δt is the time interval (t_n, t_{n+1}).

4.5 Stream function

The understanding of flow structures is an essential component of fluid dynamics analysis. In a two-dimensional coordinate system, stream functions can be used to calculate flow structure, providing valuable quantitative insights. For each dimensional face of a three-dimensional coordinate system, multiple stream functions are required. Stream functions serve as powerful tools for illustrating flow structure, conveying important physical meaning, and facilitating mathematical analysis. Streamlines are used to interpret the solid boundaries of a flow by representing its flow field in relation to local velocity vectors. In particular, they are useful for assessing recirculation regions quantitatively. The generation of stream functions becomes essential when simulating fluid flow problems using primitive variables. Using this technique to visualize the flow pattern in a clear and concise manner. The stream function must be understood prior to drawing streamlines from one node position to another. A family of curves that traverse the flow structure can be calculated from the velocity gradient and can describe the stream function. The variation of fluid particles along a single streamline or path line within a steady-state flow field remains constant. The stream function complies with Poisson's equation in Cartesian and cylindrical polar coordinates systems. In the case of incompressible two-dimensional flow, an appropriate vector potential, denoted as 'Ψ' as follows:

$$V = \nabla \times \Psi. \tag{32}$$

Where, $\Psi = (0, 0, \Psi)$ represents the stream function. Since Cartesian coordinates in the computation are a subclass of axisymmetric frames of reference, we will only discuss an axisymmetric frame of reference here. Assume the components of velocity are in the radial and axial directions of an axisymmetric cylindrical polar coordinate system (r,z). Stream function $\Psi(r, z)$ and velocity components fulfill the following relationships [3].

$$\frac{1}{r}\frac{\partial \Psi}{\partial r} = -v_z \quad and \quad \frac{1}{r}\frac{\partial \Psi}{\partial z} = v_r. \tag{33}$$

This scheme is obtained by using a pseudo-time stepping procedure in equation (33):

$$\frac{\partial \Psi}{\partial t} = \left(\frac{\partial^2 \Psi}{\partial r^2} + \frac{\partial^2 \Psi}{\partial z^2}\right) - r\frac{\partial v_z}{\partial r} - v_z + r\frac{\partial v_r}{\partial z}. \tag{34}$$

After dividing by r gives, equation (34) becomes:

$$\frac{1}{r}\frac{\partial \Psi}{\partial t} = \frac{1}{r}(\nabla^2 \Psi) - \frac{\partial v_z}{\partial r} - \frac{v_z}{r} + \frac{\partial v_r}{\partial z}. \tag{35}$$

For time derivative equation (35) using the forward time stepping approach along (Δt) step, the different configuration of equation (35) develops:

$$\frac{1}{r}\left(\frac{\Psi^{n+1} - \Psi^n}{\Delta t}\right) = \frac{1}{r}(\nabla^2 \Psi^n) - \frac{\partial v_z}{\partial r} - \frac{v_z}{r} + \frac{\partial v_r}{\partial z}. \tag{36}$$

Utilizing the weighted residual technique, a weak form of equation (36) turn into:

$$\frac{1}{\delta t}\int_\Omega \frac{w}{r}(\Psi^{n+1} - \Psi^n) r d\Omega = \int_\Omega \frac{w}{r}(\nabla^2 \Psi^n) r d\Omega - \int_\Omega w\frac{\partial v_z}{\partial r} r d\Omega - \int_\Omega w\frac{v_z}{r} r d\Omega + \int_\Omega w\frac{\partial v_r}{\partial z} r d\Omega. \tag{37}$$

A finite element approximation will be:

$$(\Psi, v_r, v_z) = \Sigma_{i=1}^{N}(\Psi_j, V_r^j, V_z^j)\Phi_i(r, z). \tag{38}$$

Stream function Ψ'_j, radial, and axial velocity components are characterized by (V_r^j, V_z^j) in r and z-direction respectively for on j nodal point. The Galerkin Approximation is based on a finite element approach in which the weight function (w_i) is assumed to be equivalent to the shape function (Φ_i) and is shown in the following figure [3]:

$$\Sigma_{i=1}^{N} w_i(x) = \Sigma_{i=1}^{N} \Phi_i(x). \tag{39}$$

Gives:

$$\frac{1}{\Delta t}\int_{\Omega} \Phi_i \Phi_j d\Omega \Delta \Psi_j^{n+1} = \int_{\Omega} \Phi_i(\nabla^2 \Phi_j) d\Omega \Psi_j^n - \int_{\Omega} \Phi_i \frac{\partial \phi_j}{\partial r} r d\Omega v_z^j - \int_{\Omega} \Phi_i \Phi_j d\Omega v_z^j + \int_{\Omega} \Phi_i \frac{\partial \Phi_j}{\partial z} r d\Omega v_r^j. \tag{40}$$

The Dirichlet boundary conditions are used, in terms to reduce second-order derivatives of (40) by integrating by parts and neglecting the boundary integrals through Green's theorem:

$$\frac{1}{\Delta t}\int_{\Omega} \Phi_i \Phi_j d\Omega \Delta \Psi_j^{n+1} = -\int_{\Omega} \frac{\partial \Phi_i}{\partial r}\frac{\partial \Phi_j}{\partial r}\frac{\partial \Phi_i}{\partial z}\frac{\partial \Phi_j}{\partial z} r d\Omega \Psi_j^n - \int_{\Omega} \Phi_i \frac{\partial \Phi_j}{\partial r} r d\Omega v_z^j - \int_{\Omega} \Phi_i \Phi_j d\Omega v_z^j + \int_{\Omega} \Phi_i \frac{\partial \Phi_j}{\partial z} r d\Omega v_r^j. \tag{41}$$

According to matrix-vector notation, the above equation (41) is expressed explicitly and semi-implicitly as follows:

$$\frac{1}{\Delta t} M \Delta \Psi_j^{n+1} = -S\Psi_j^n - D_1 v_z^j - M v_z^j + D_2 v_r^j, \tag{42}$$

$$\left(\frac{1}{\Delta t} M + \frac{S}{2}\right) \Delta \Psi_j^{n+1} = -S\Psi_j^n - D_1 v_z^j - M v_z^j + D_2 v_r^j. \tag{43}$$

Where M is mass like a matrix with entries $\int_{\Omega} \Phi_i \Phi_j d\Omega$ and S is known as a diffusion-like term in a matrix with entries:

$$\int_{\Omega} \frac{\partial \Phi_i}{\partial r}\frac{\partial \Phi_j}{\partial r} + \frac{\partial \Phi_i}{\partial z}\frac{\partial \Phi_j}{\partial z} d\Omega$$

In equations (42 and 43), D_1 and D_2 denoted as velocity gradient matrices with entries: $\int \Phi_i \frac{\partial \Phi_j}{\partial r} r d\Omega$ and $\int \Phi_i \frac{\partial \Phi_j}{\partial z} r d\Omega$.

5 Results and discussion

The meshing of the flow domain was accomplished using uniform conformal mappings, a technique that automatically aligned the sides of the elements with the streamlines and maintained the orthogonality of the elements. This flow analysis examined the influence of inertia on the flow structure, examined the effect of flow rate changes, examined pressure differences caused by the flow, and considered the influence of porosity within the computational domain. Using the stream function, the length of vortices and intensity of flow recirculation were calculated at different Reynolds numbers. Reynolds numbers increased, and the results were presented using stream functions, including the pressure difference at the inlet. At various axial positions, including the axis of symmetry, velocity profiles were specified. To understand vortex formation in different flow structures, it is imperative to determine critical Reynolds numbers. This can be achieved by varying the flow rate. Vortex formation was investigated using Reynolds number ranges of $(1 \leq Re \leq 200)$ for flows in non-porous media and $(1 \leq Re \leq 5000)$ for Newtonian fluid flows in pipes containing both non-porous and porous media.

5.1 Mixing and Separation Phenomena in Newtonian Flows within a Pipe

The specific problem involving combined mixing and separating flows is depicted in Figure 1 (a). Numerical solutions are provided for various flow rates and flow directions, achieved by rising the Reynolds number. The focus of the investigation lies in understanding the influence of inertia, vortex size, and vortex intensity when a non-porous and porous material fills the channel. Through numerical simulations, we analyze the results by visualizing streamlined patterns and the filled domain. We aim to examine the effects of altering flow rates, varying materials, and the influence of porous media on the development, intensity, and enhancement of vortices, as well as the resulting pressure difference. Furthermore, compute the pressure difference at the inlet as a function of Reynolds number.

5.2 Newtonian Behavior and Analysis of flow in non-porous media filled pipes

The presence of flow patterns characterized by a combined-separating formation is a significant aspect that can indicate stagnant regions and overall progress in a system. In Figures 2 to 3, Newtonian fluid flows are shown in a pipe filled with non-porous media, along with streamlined projections. The objective of this section is to simulate Newtonian fluids in a combined-separating domain numerically. Through the analysis of streamlined patterns, we examine the influence of inertia. We examine vortex growth and explore the impact of changing flow rates on flow structure.

5.3 Equal (1, 1) flow rate

When the flow rate is equal, the maximum velocities at the center of the domain $V_1 = V_2$ are also equal. The influence of fluid inertia on flow behavior is examined through streamlined projections, as shown in Figure 2. By varying the inertia using Reynolds numbers ranging from Re = 1 to 200, it has been observed that the flow responds to the presence of a gap, leading to flow disruption. Some of the flow becomes unidirectional, while mixing occurs within the gap, and the flow merges at both the upper and lower exits of the domain (Re = 1). At an equal flow rate of (1, 1), no significant vortex generation is observed in the center of the domain, even at high Reynolds numbers. The overall flow structure remains similar in all cases, except for the redirection of flow towards the line of symmetry within the internal pipe. This particular flow phenomenon does not yet fully understood.

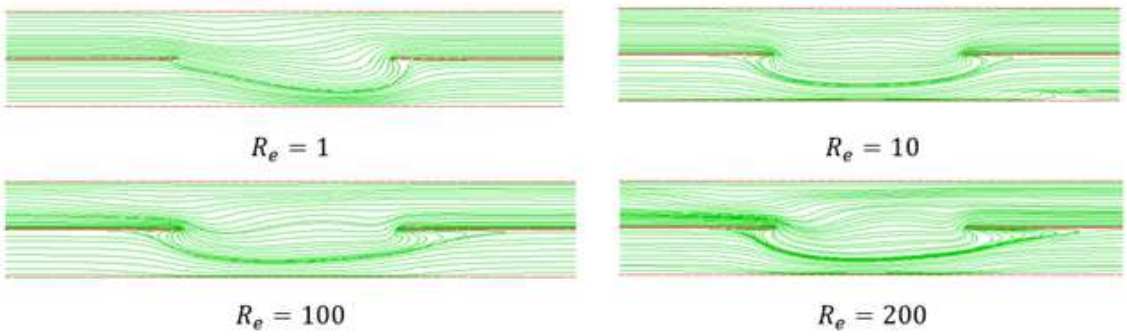

Figure 2. In a pipe filled with a non-porous medium, a Newtonian mixing and separating flow of equal (1, 1) flow rate is shown with an increase in Re from top to bottom.

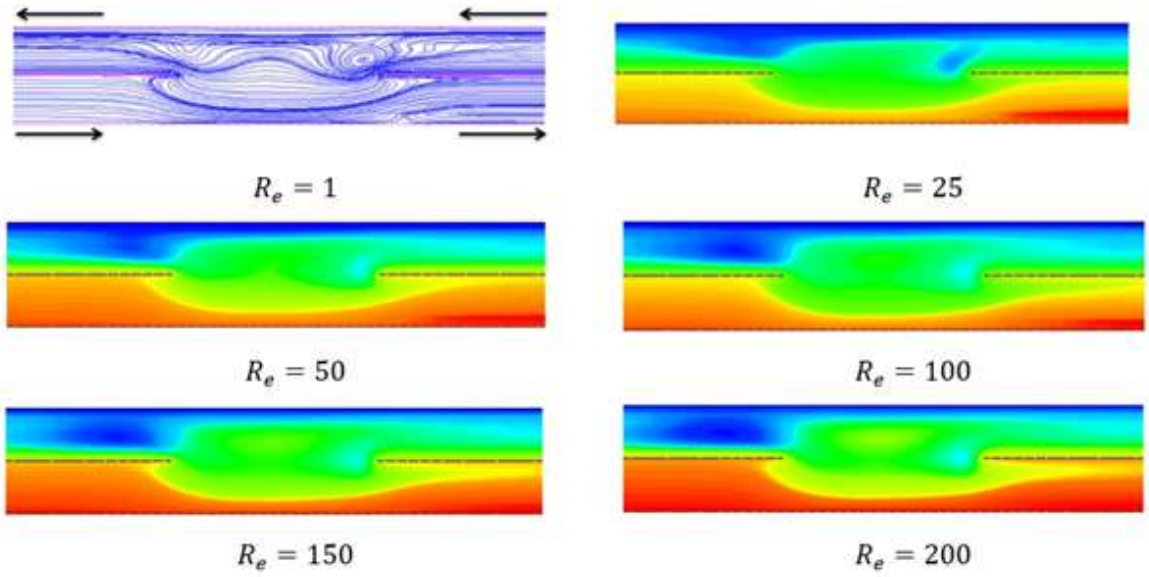

Figure 3. Analyzing Newtonian mixing-separating flow in a non-porous medium: Reversing Reynolds number gradients in a pipe.

5.4 Influence of flow rate

5.5 Unequal (1, 2) flow rate

The purpose of this study is to examine the impact of inertia on the flow behavior of a Newtonian fluid. Numerical simulation was performed by varying the Reynolds number (Re) between 1 and 200, as shown in Figure 3. The purpose of the analysis was to gain insight into the flow phenomena that occur when flow rates change from being equal to unequal in the inner and outer pipes. Specifically, the decision was made to set up a double flow rate in the outer pipe, flowing in the opposite direction. Even at a low Reynolds number of 1, an intriguing flow phenomenon was observed. There was a distinct recirculating region near the separating region of the outer pipe, as depicted in Figure 3. The vortex activity intensified as the

Reynolds number exceeded 1 and extended further into the center of the domain. There were vortices observed upstream from the right and left sides of the outer pipe. As the Reynolds number approached 50, the central vortex shifted downward within the pipe, and two additional vortices formed: a strong vortex in the middle gap of the domain, slightly above the central gap, and a second vortex downstream of the outer cylinder. As the Reynolds numbers increased up to 200, these three vortices became more prominent and stable. Due to the presence of a vortex in the gap, fluid from the inlet was pushed toward the inner pipe. Consequently, the vortex near the plate was pushed into the inner pipe due to the double flow rate in the outer cylinder. Flows were primarily mixed within the inner pipe by redirecting them toward the line of symmetry. In Figures 2 and 3, we show the results obtained for Newtonian fluids flowing at equal (1, 1) and unequal (1, 2) flow rates. It was observed that altering the flow rate in the outer cylinder significantly increased the intensity and enhancement of vortices in both the outer cylinder and the separation gap within the domain. In the case of unequal flow rates, the fluid was pushed down into the separation gap of the inner pipe, directing it toward the line of symmetry. This double-flow arrangement led to mixing occurring exclusively within the inner pipe.

5.6 Analysis of the impact of flow rates and inertia on pressure

The pipe filled with a nonporous medium with Newtonian mixing and separating of fluids is shown in Figure 4.

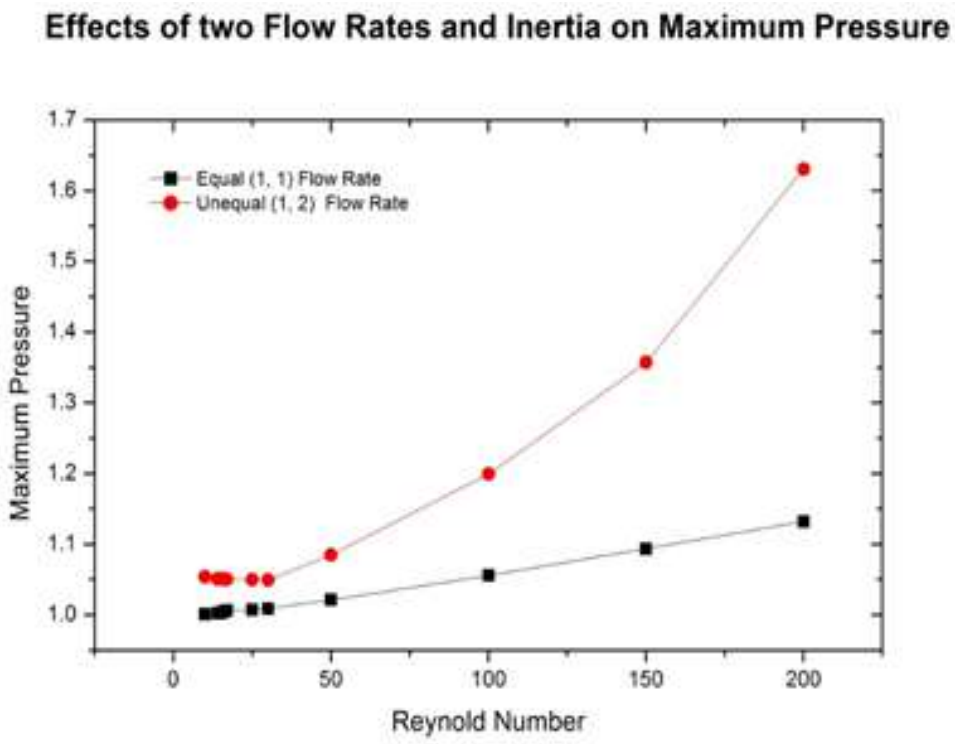

Figure 4. In Pipes filled with non-porous media, maximum-scaled pressure is compared to inertia at different flow rates

In Newtonian fluid flows, nondimensional scaled pressures are obtained in inner and outer pipes filled with nonporous media is $1 \leq p_s \leq 1.132$ and $1 \leq p_s \leq 1.6309$ under both equal (1, 1) and unequal (1, 2) conditions. Pressure increases because of varying flow rate and increasing inertia. Vortex development was more frequent in channel flows than in pipe flows. The pressure increase is less for initial values of Re from 1 to 50 than for initial values of Re from 100 to 200. When flow rates are equal, growth is linear, but when flow rates are doubled, the increase in scaled pressure is nonlinear.

5.7 Newtonian Fluid Flows in Porous Media: Mixing and Separation

Fig. 1 (a) illustrates the details of the investigated combined mixing and separating flow problem, focusing on the saturated porous media domain. A Newtonian fluid flow through porous media is analyzed using streamline projections across a wide range of Reynolds numbers, ranging from Re=1 to 5000. This study examined both equal and unequal flow rates. The effect of various parameters on flow behavior and characteristics has been thoroughly discussed. Under different flow rates in pipes filled with porous media, the research seeks to provide comprehensive insights into the interaction between maximum scaled pressure and inertia. It is anticipated that the findings of this study will contribute to a better understanding of fluid flow phenomena in porous media, and will provide valuable information for the design and optimization of flow systems involving porous media domains.

5.8 Analyzing the Disparity in Flow Rates: Understanding Equal (1, 1) Flow Rate Phenomena

This study investigates the effect of the Reynolds number on the flow characteristics in a pipe filled with porous media. The focus of this paper is on Newtonian fluids, and Figure 5 illustrates the corresponding numerical results.

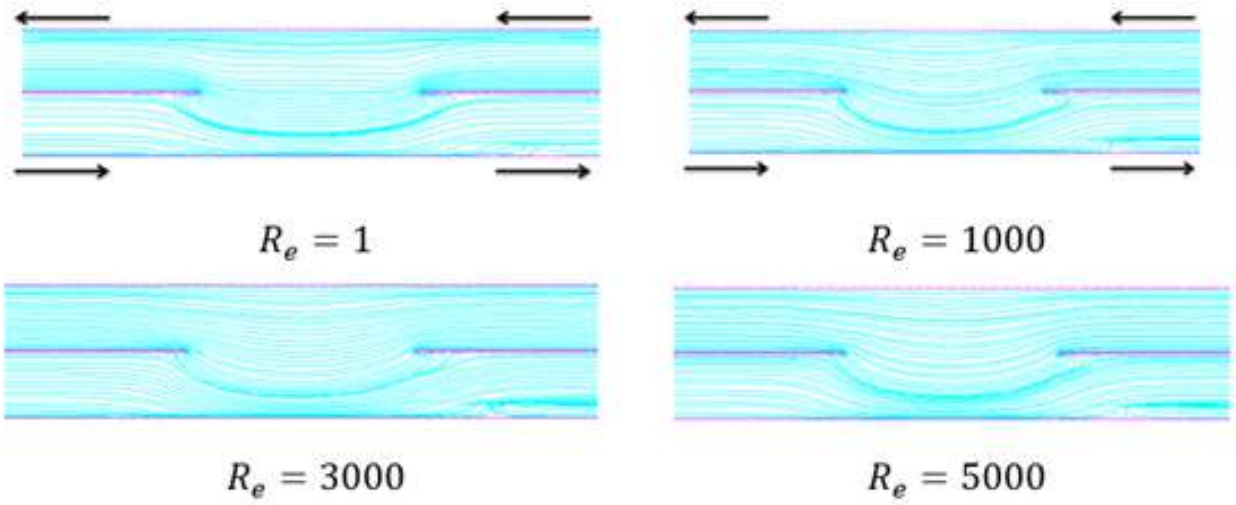

Figure 5. Streamline Newtonian combined mixing and separating flow in a porous medium-filled pipe filled with an equal flow rate (1, 1) as Re increases from top to bottom

The development of vortices within the system is not noticeable at equal flow rates. Fluid exits the inlet

cylinder and enters the central pipe, returning to the same cylinder downstream. It is important to note that this behavior differs from flows without porous materials, where mixing is usually observed. The fluid flow in porous media is primarily directed towards the line of symmetry as the Reynolds number increases. Figure 5 illustrates the flow structure and indicates that there is no significant inertial effect. Due to this, only a limited number of simulated results are presented, namely for Reynolds numbers ranging from 1 to 5000.

5.9 Analysing the Disparity in Flow Rates: Understanding Unequal (1, 2) Flow Rate Phenomena

Figure 6 illustrates a simulation of Newtonian fluids flowing within a porous media domain, spanning a range of Reynolds numbers from 1 to 5000. The absence of vortex formation indicates a lack of mixing in comparison with flows unimpeded by porous materials. Further investigation is required to determine whether there is an artifact present in the inner pipe caused by the double flow rate in the outer cylinder. As shown in Figure 5, the fluid flow within the inner pipe was primarily downward.

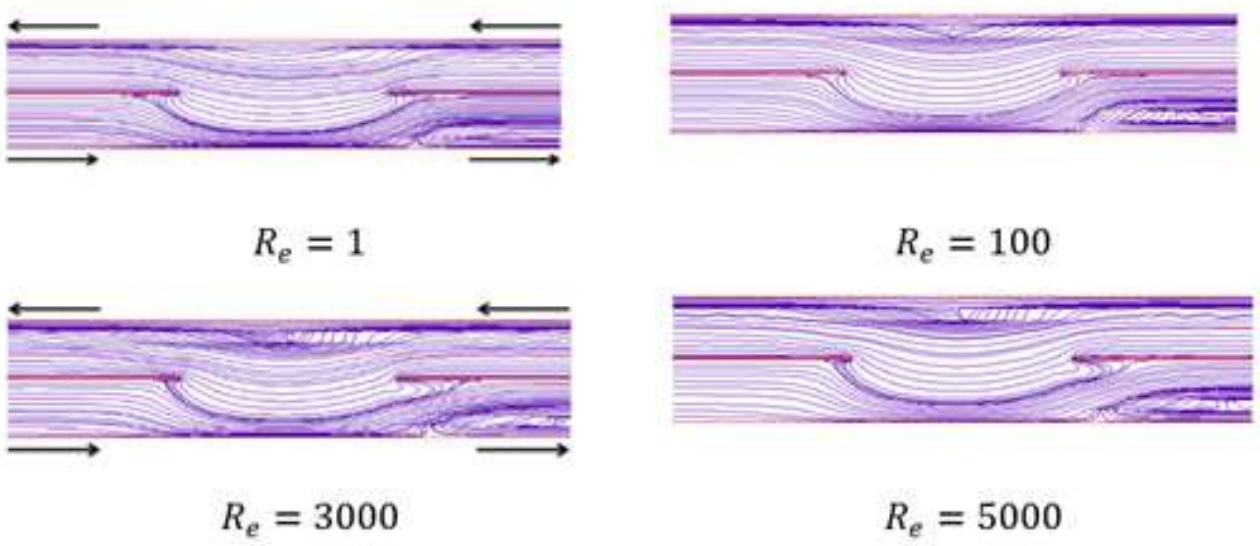

Figure 6. Newtonian Flow Optimization in Porous Media: Streamlining Mixing and Separation With Varying Flow Rates (1, 2)

5.10 Influence of flow rate

Figures (5 to 6) demonstrate the results for both equal (1, 1) and unequal (1, 2) flow rates in the computational domain. In numerical simulations, there is no dramatic change in flow rate in the outer wall of the cylinder when the flow rate is reversed. When the flow rate is unequal, the fluid is forced down into a separation gap of the inner pipe and then returned to the upstream of the outer cylinder. Changing the flow rate in the outer cylinder did not result in any mixing effects. The inner pipe has been found to contain some numerical artifacts, which will be examined in future studies.

5.11 Effects of flow rates and permeability on Pressure

A numerical simulation of Newtonian fluid flow in a porous pipe is illustrated in Figure 7, the trends observed under two different flow rates, increasing Reynolds numbers, and varying values of permeability can be viewed. Scaled pressures range from a minimum of $1 \leq p_s \leq 991.8812$ to a maximum of $1 \leq p_s \leq 683.5631$ for unequal and equal flow rates, respectively. As a result of adjusting the permeability values, a significant variation in pressure can be observed when comparing equal and unequal flow rates. The pressure is consistently increased with varying flow rates, regardless of whether the pipe is filled with porous media or not, with the exception of one particular section where the opposite trend is observed. The inclusion of Darcy's effects in the computational domain results in a rapid increase in pressure compared to Newtonian fluid flows without porous media. It is observed that, in this setting, the value of κ (permeability) ranges from 0.00001 to 0.001 for unequal and equal flow rates from $0.001 \leq \kappa \leq 0.00001$, and $0.01 \leq \kappa \leq 0.00001$ respectively. Forchheimer's number remains constant at 0.0001 for unequal flow rates and 0.001 for equal flow rates. As flow rates and inertia vary, the impact of changes in permeability and Forchheimer number on pressure is evident. Changing the permeability value results in significant pressure variations when the Reynolds number ranges between 1 and 4000. In contrast, when the Reynolds number ranges between 4000 and 10000, the permeability remains constant, resulting in a linear pressure trend.

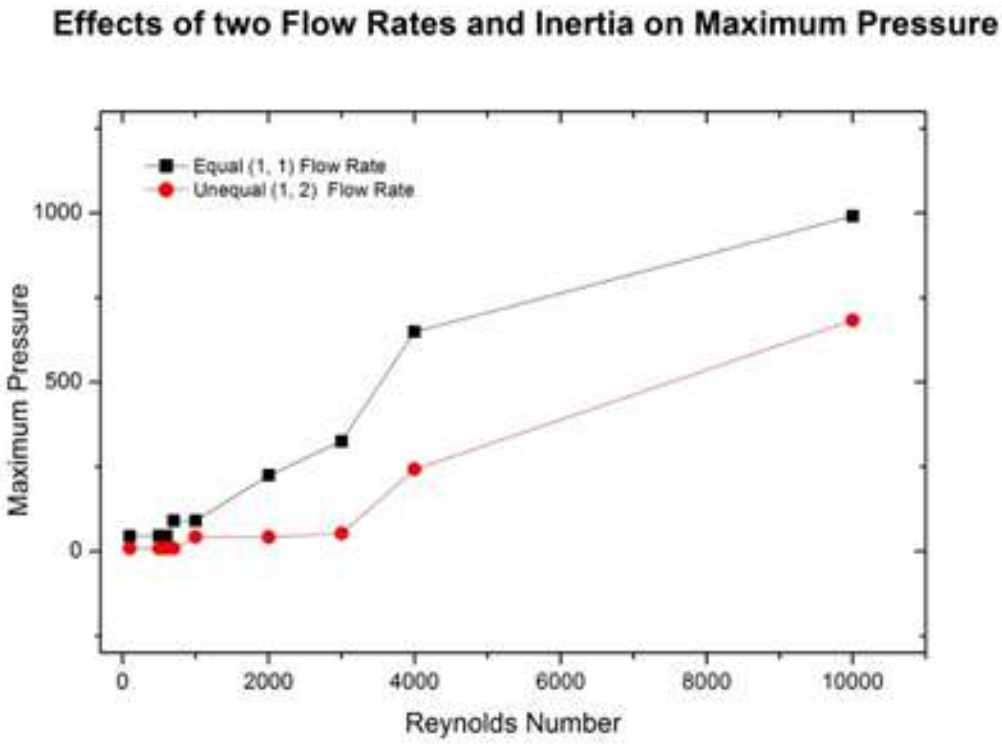

Figure 7. A comparative study of the effects of porous media on maximum-scaled pressure and inertia in pipes at varying flow rates.

6 Conclusion

The conclusion of the above study can be summarized as follows:

- The numerical simulations of Newtonian fluids in pipe systems, both with and without porous media, provide valuable insights into the behavior of combing and separating flows.
- Vortex development is significantly influenced by the change in flow rates in the outer cylinder of the pipe system. There are vortices observed in the separation gap near the central plate and downstream of the outer cylinder.
- The presence of porous media in the inner pipe has an effect on fluid flow, pushing it down towards the line of symmetry, but does not result in significant vortex formation.
- Increasing the Reynolds number leads to the growth and stability of vortices, particularly in the outer cylinder and the separation gap.
- Pressure differences are evidently affected by changes in flow rates, inertia, Darcy's number, and permeability. Inertia and flow rate increase pressure with increasing inertia, and equal or unequal flow rates have significant effects on pressure.
- The study highlights the importance of considering factors such as flow rates, porous media, and Reynolds number in the design and optimization of pipe systems for various engineering applications.

Overall, this study contributes to the understanding of fluid dynamics in pipe systems and provides insights that can be applied in engineering design and optimization processes.

References

[1] A. M. Afonso, M. A. Alves, R. J. Poole, P. J. Oliveira, and F. T. Pinho, "Viscoelastic flows in mixing-separating cells," J. Eng. Math., vol. 71, pp. 3–13, 2011.

[2] S. O. S. Echendu, F. Belblidia, H. R. Tamaddon-Jahromi, and M. F. Webster, "Modelling with viscous and viscoplastic materials under combining and separating flow configurations," Mech. Time-Dependent Mater., vol. 15, pp. 407–428, 2011.

[3] A. Baloch, P. Townsend, and M. F. Webster, "On the simulation of highly elastic complex flows," J. Non-newton. Fluid Mech., vol. 59, no. 2–3, pp. 111–128, 1995.

[4] R. B. Khokhar, "Numerical Modelling of Mixing and Separating of Fluid Flows through Porous Media," 2018.

[5] Bhutto, A. A., M. Hussain, S. F. Shah, and K. Harijan. "Computation of Vortex Driven Flow Instability through Unsteady RANS and Scale Resolving Simulation." Institute of Space Technology 12, no. 1 2022: 14-22.

[6] Memon, K. N., Sher Afzal Khan, S. Islam, Nazir Ahmad Zafar, Syed Feroz Shah, and A. M. Siddiqui. "Unsteady drainage of electrically conducting power law fluid." Applied Mathematics and Information Sciences 8, no. 5 2014: 2287.

[7] B. Xia and D.-W. Sun, "Applications of computational fluid dynamics (CFD) in the food industry: a review," Comput. Electron. Agric., vol. 34, no. 1–3, pp. 5–24, 2002.

[8] Bhutto, Afaque Ahmed, Iftikhar Ahmed, Saeed Ahmed Rajput, and Syed Asad Raza Shah. "The effect of oscillating streams on heat transfer in viscous magnetohydrodynamic MHD fluid flow." 2023.

[9] Memon, K. N., S. Islam, A. M. Siddiqui, Sher Afzal Khan, Nazir Ahmad Zafar, and M. Akram. "Lift and drainage of electrically conducting power law fluid on a vertical cylinder." Applied Mathematics and Information Sciences 8, no. 1 (2014): 45.

[10] F. P. T. Baaijens, "Mixed finite element methods for viscoelastic flow analysis: a review," J. Nonnewton. Fluid Mech., vol. 79, no. 2–3, pp. 361–385, Nov. 1998, doi: 10.1016/S0377-0257(98)00122-0.

[11] Bhutto, Iftikhar Ahmed, Afaque Ahmed Bhutto, Rahim Bux Khokhar, Muhammad Aslam Soomro, and Fozia Shaikh. "The effect of uniform and exponential streams on Magnetohydrodynamic flows of viscous fluids." 2023.

[12] Memon, K. N., A. M. Siddiqui, and S. F. Shah. "Exact solution of tank drainage for Newtonian fluid with slip condition." Sindh University Research Journal (Science Series) 49, no. 2 (2017): 283-288.

[13] M. Fortin and D. Esselaoui, "A finite element procedure for viscoelastic flows," Int. J. Numer. Methods Fluids, vol. 7, no. 10, pp. 1035–1052, 1987, doi: 10.1002/FLD.1650071004.

[14] T. Cochrane, K. Walters, and M. F. Webster, "Newtonian and non-Newtonian flow near a re-entrant corner," J. Nonnewton. Fluid Mech., vol. 10, no. 1–2, pp. 95–114, 1982.

[15] A. A. Bhutto, S. F. Shah, R. B. Khokhar, K. Harijan, and M. Hussain, "To Investigate Obstacle Configuration Effect on Vortex Driven Combustion Instability," 2023.

[16] A. A. Bhutto, K. Harijan, M. Hussain, S. F. Shah, and L. Kumar, "Numerical simulation of transient combustion and the acoustic environment of obstacle vortex-driven flow," Energies, vol. 15, no. 16, p. 6079, 2022.

[17] B. Alazmi and K. Vafai, "Analysis of fluid flow and heat transfer interfacial conditions between a porous medium and a fluid layer," Int. J. Heat Mass Transf., vol. 44, no. 9, pp. 1735–1749, 2001.

[18] M. A. Al-Nimr and T. K. Aldoss, "The effect of the macroscopic local inertial term on the non-Newtonian fluid flow in channels filled with porous medium," Int. J. Heat Mass Transf., vol. 47, no. 1, pp. 125–133, 2004.

[19] K. Walters and M. F. Webster, "On dominating elastico-viscous response in some complex flows," Philos. Trans. R. Soc. London. Ser. A, Math. Phys. Sci., vol. 308, no. 1502, pp. 199–218, 1982.

[20] T. Cochrane, K. Walters, and M. F. Webster, "On Newtonian and non-Newtonian flow in complex geometries," Philos. Trans. R. Soc. London. Ser. A, Math. Phys. Sci., vol. 301, no. 1460, pp. 163–181, 1981.

[21] A. Afonso, M. A. Alves, R. J. Poole, P. J. Oliveira, and F. T. Pinho, "Viscoelastic low-Reynolds-number flows in mixing-separating cells," 2008.

[22] K. Dharejo, H. Shaikh, B. Shah, and A. Baloch, "Least square Galerkin Finite Element study of Newtonian Fluids Flow through channel with fixed Rectangular Single Baffle," Sindh Univ. Res. Journal-SURJ (Science Ser., vol. 50, no. 2, pp. 215–220, 2018.

[23] D. M. Hawken, H. R. Tamaddon-Jahromi, P. Townsend, and M. F. Webster, "A Taylor–Galerkin-based algorithm for viscous incompressible flow," Int. J. Numer. Methods Fluids, vol. 10, no. 3, pp. 327–351, 1990.

[24] F. T. Pinho and P. J. Oliveira, "Analysis of forced convection in pipes and channels with the simplified Phan-Thien–Tanner fluid," Int. J. Heat Mass Transf., vol. 43, no. 13, pp. 2273–2287, 2000.

[25] R. I. Tanner, "Constitutive model for 7th Workshop on Numerical Computations in Viscoelastic Flows," 1989.

[26] H. Benzenine, R. Saim, S. Abboudi, and O. Imine, "Numerical simulation of the dynamic turbulent flow field through a channel provided with baffles: comparative study between two models of baffles: transverse plane and trapezoidal," J. Renew. Energies, vol. 13, no. 4, pp. 639–651, 2010.

[27] J. Donea, "A Taylor–Galerkin method for convective transport problems," Int. J. Numer. Methods Eng., vol. 20, no. 1, pp. 101–119, 1984.

[28] C. Cuvelier, A. Segal, and A. A. Van Steenhoven, Finite element methods and Navier-Stokes equations, vol. 22. Springer Science and Business Media, 1986.

[29] C. Johnson, A. Szepessy, and P. Hansbo, "On the convergence of shock-capturing streamline diffusion finite element methods for hyperbolic conservation laws," Math. Comput., vol. 54, no. 189, pp. 107–129, 1990.

[30] A. J. Chorin, "Numerical solution of the Navier-Stokes equations," Math. Comput., vol. 22, no. 104, pp. 745–762, 1968.

[31] R. Peyret and T. D. Taylor, "Computational methods for fluid flow," Il.

[32] J. Van Kan, "A second-order accurate pressure-correction scheme for viscous incompressible flow," SIAM J. Sci. Stat. Comput., vol. 7, no. 3, pp. 870–891, 1986.

[33] O. C. Zienkiewicz and R. Codina, "A general algorithm for compressible and incompressible flow—Part I. The split, characteristic-based scheme," Int. J. Numer. methods fluids, vol. 20, no. 8-9, pp. 869–885, 1995.

[34] O. C. Zienkiewicz, R. L. Taylor, and R. L. Taylor, The finite element method: solid mechanics, vol. 2. Butterworth-heinemann, 2000.

[35] X.-D. Liu and P. D. Lax, "Positive schemes for solving multi-dimensional hyperbolic systems of conservation laws," Sel. Pap. Vol. I, pp. 337–360, 2005.

[36] G. A. Sod, "A survey of several finite difference methods for systems of nonlinear hyperbolic conservation laws," J. Comput. Phys., vol. 27, no. 1, pp. 1–31, 1978.

[37] E. O. Carew, P. Townsend, and M. F. Webster, "Taylor-Galerkin algorithms for viscoelastic flow: application to a model problem," Numer. Methods Partial Differ. Equ., vol. 10, no. 2, pp. 171–190, 1994.

[38] J. Donea, "Recent advances in computational methods for steady and transient transport problems," Nucl. Eng. Des., vol. 80, no. 2, pp. 141–162, 1984.

[39] M. A. Solangi, R. B. Khokhar, and A. Baloch, "A fem study for non-newtonian behaviour of blood in plaque deposited capillaries: Analysis of blood flow structure," Mehran Univ. Res. J. Eng. Technol., vol. 32, no. 2, pp. 277–282, 2013.

[40] D. Solangi, H. Shaikh, R. B. Khokhar, and A. Baloch, "Numerical study of Newtonian blood flow through a plaque deposited artery," Sindh Univ. Res. J. (Science Ser., vol. 45, no. 01, pp. 79–82, 2012.